New γ-ray measurements for $^{12}C + ^{12}C$ sub-Coulomb fusion: Toward data unification

E. F. Aguilera,[1,2] P. Rosales,[1] E. Martinez-Quiroz,[1] G. Murillo,[1,2] M. Fernández,[1] H. Berdejo,[1] D. Lizcano,[1] A. Gómez-Camacho,[1] R. Policroniades,[1] A. Varela,[1] E. Moreno,[1] E. Chávez,[3] M. E. Ortíz,[3] A. Huerta,[3] T. Belyaeva,[2] and M. Wiescher[4]

[1]*Departamento del Acelerador, Instituto Nacional de Investigaciones Nucleares, Apartado postal 18-1027, C.P. 11801, México D.F., México*

[2]*Universidad Autónoma del Estado de México, C.P. 50000, Toluca, México*

[3]*Instituto de Física, Universidad Nacional Autónoma de México, Apartado postal 20-364, C.P. 01000, México, D.F., México*

[4]*Department of Physics & Joint Institute for Nuclear Astrophysics, University of Notre Dame, Notre Dame, Indiana 46556, USA*

(Received 14 December 2005; published 13 June 2006)

Fusion excitation functions are measured for the α, p, and n evaporation channels in the fusion of the $^{12}C + ^{12}C$ system at center-of-mass energies between 4.42 and 6.48 MeV, with energy steps of 75 keV. The γ-ray technique is used with a new absolute normalization method which is independent of charge collection, allowing one to monitor at the same time the carbon buildup at the target. Discrepancies between previous works are discussed and a simple unification is proposed. Barrier penetration model (BPM) calculations are consistent with a belly-to-belly orientation of the oblate deformed ^{12}C nuclei at the touching point. As in previous works, much structure is seen in the excitation function which is nearly consistent with the positions of resonances reported in the literature for this system. Using BPM predictions for the background excitation function and doing a simultaneous fit of the relevant Breit-Wigner terms in the measured energy region produced a modified set of resonance parameters. The extrapolation of the astrophysical S factor to lower energies is discussed on the basis of the unified data.

DOI: 10.1103/PhysRevC.73.064601 PACS number(s): 25.60.Pj, 25.70.Gh, 25.70.Ef

I. INTRODUCTION

The discovery in 1960 that the excitation functions for the elastic [1] and reaction channels [2] in the $^{12}C + ^{12}C$ system presented unexpected resonant structure was the trigger for a virtual explosion of experimental and theoretical studies aimed at understanding the underlying phenomena. After more than four decades, this system stands out as one of the most interesting subjects to study because of at least three reasons. First, this is the system where more evidence for quasimolecular structure has been found, coming mainly from excitation function measurements for many of the possible reaction channels [1–14]. In spite of the many attempts to describe the observations, reviewed, for example, in Ref. [14], the vast amount of data accumulated in this respect still awaits a sound theoretical model capable of explaining all the observed details. Second, systematic optical-model analyses of the elastic channel for this system, which has been measured in a wide $E_{\text{c.m.}}$ range going from a few MeV to around 725 MeV, have provided the best evidence that the whole energy region can be consistently described with nearly unified optical potentials using deep real parts [15–17]. In the lowest energy region, however, it has been found recently [18] that the additional constraints imposed by the experimental fusion cross sections seem to require optical potentials with more complex geometries than the simple Woods-Saxon or Woods-Saxon-squared shapes usually assumed. Finally, there is currently a keen astrophysical interest in the fusion channel in the low-energy region because of its critical role in studying a wide range of stellar burning scenarios in carbon-rich environments [19–23]. Indeed, this reaction is important to the understanding of the carbon-burning nucleosynthesis which presumably occurs in massive stars in the late stages of stellar evolution [19–21], in accreting neutron stars [22,23], and in exploding white dwarfs producing type Ia supernovae [23].

The fusion-evaporation channel has been measured at sub-Coulomb energies as low as around $E_{\text{c.m.}} = 2.5$ MeV [9,24,25], or $E_{\text{c.m.}} = 3$ MeV [11,26], which is near but still at the top of the region of astrophysical interest (1–3 MeV). Measurements at lower energies are extremely difficult, and the extrapolation from current data to this region is complicated because of two main reasons. First, the resonant structures observed even in the low-energy part of the excitation function make unreliable any extrapolation using the statistical model; and second, the various data sets available up to now show considerable discrepancies, as illustrated with the data shown in Fig. 1 for energies between 4.5 and 6.5 MeV. With cross section values still not too difficult to measure, between 1 and 200 mb, this energy region is critical to determining a reliable absolute normalization, which in an excitation function measurement is then carried down to the lower energies. However, there are clear discrepancies in absolute values between these data sets, which in some cases amount to factors of about 3 and certainly fall far from the reported uncertainties. It is worthwhile to specify that five of these works [7,9,12,25,27] measured secondary γ rays from the evaporation residues; the other three [11,24,26] obtained their results by detecting the evaporated particles. No evidence seems to exist in these data of a possible systematic difference directly related to the measurement technique.

In addition, even though the observed structure is qualitatively similar for the different experiments, there are clear shifts in energy between some of the data sets, indicating that the experimental control of this quantity might be harder than

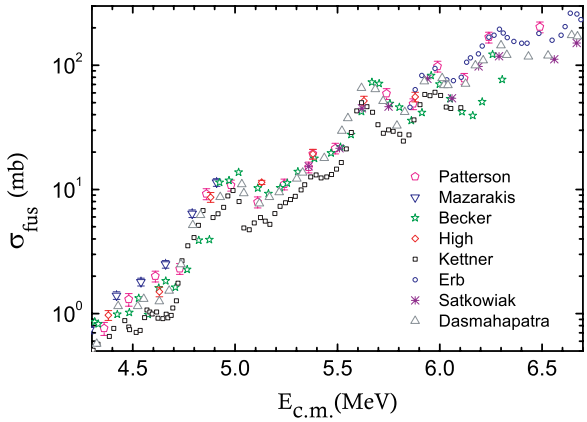

FIG. 1. (Color online) Comparison of some experimental fusion excitation functions for $^{12}C + {}^{12}C$ in the region between 4.4 and 6.5 MeV. Data are from [7,9,11,12,24–27].

first thought. An undetected carbon buildup on the target, for example, would not only affect the absolute normalization factor but also produce a shift in the effective reaction energy. Since the buildup takes place only at the beam spot and increases with the beam fluence at the target [28–30], an on-line monitoring of the target thickness at the beam spot is necessary along the whole experiment in order to guarantee correct results. Such a monitoring has never been attempted, although buildup corrections have been estimated by repetition of measurements at selected beam energies [7]. At far subbarrier energies, however, frequent repetition becomes unpractical. In addition, it is critical that repetition measurements be done with the beam hitting precisely the same target spot, a goal that may not be easy to achieve in all situations. We must also mention that in some cases, very careful provisions were taken to minimize the carbon buildup at the target [11,12], even though actual monitoring was not done.

For these kinds of measurements, where considerable structure is expected, it is desirable to take data with small energy steps, which requires using rather thin targets. This fact, combined with the low cross section values at sub-Coulomb energies, necessarily produces low yields of reaction products. The γ-ray technique has the advantage that large solid angles may be covered, thus reducing the counting time for a given statistic and a particular beam current. One disadvantage is that the absolute normalization of the cross sections usually relies heavily on collecting the beam charge, a task that the undesirable secondary electrons render rather hard to accomplish with good precision. The data are thus usually renormalized to some independently measured value at a given energy, which is possibly one of the reasons for the observed discrepancies in the γ-ray measurements of Fig. 1.

The main goal of this work was to use an improved normalization method within the γ-ray technique, with continuous carbon-buildup monitoring, in order to get reliable absolute cross section values and corresponding reaction energies for the fusion of $^{12}C + {}^{12}C$. The purpose was to help solve some of the existing discrepancies in the important energy region displayed in Fig. 1. Preliminary results in this direction have been published elsewhere [31]. In addition, a global fit of resonances in this region will be made, and the usefulness of the barrier penetration model (BPM) in extrapolating the behavior of the excitation function to the region of astrophysical interest will be explored.

II. EXPERIMENTAL PROCEDURE

The experiment was performed with 9–13 MeV (lab.) ^{12}C ions from the EN-Tandem accelerator at the Instituto Nacional de Investigaciones Nucleares. Starting with 13 MeV, the beam energy was monotonically decreased in steps of 150 keV. The target was an amorphous C foil deposited onto a thick Ta backing so that the evaporation residues were fully stopped, thus reducing the relative number of Doppler shift events. Further details about the targets can be found in Ref. [30]. To prevent too much target thickening, three carbon foils were used in successive stages of the experiment, with repeat points taken whenever the target was changed. The original foil thicknesses were $t_1 = 19.2 \pm 0.9$ μg/cm^2,$t_2 = 22.7 \pm 1.0$ μg/cm^2, and $t_3 = 29.9 \pm 1.4$ μg/cm^2, as determined from the fits to the backscattering spectra that will be outlined below. Targets 1, 2, and 3 were used in the energy ranges 9.85–13, 9.25–9.85, and 8.95–9.25 MeV, respectively.

As shown schematically in Fig. 2, two Ge high-purity detectors placed at 125° and 55° were used to measure the secondary γ rays emitted by the evaporation residues. Measurements at these angles effectively minimize the effects of possible anisotropies in the γ radiation [32], and the comparison of spectra at the two angles permits easy identification of any Doppler shift effect. γ-ray sources of known activity of ^{137}Cs, ^{60}Co, ^{241}Am, ^{133}Ba, and ^{152}Eu were placed at the target position at the end of the experiment to determine the overall efficiency curve of the Ge detectors.

To reduce the room background, a lead shield 5 cm thick was placed around the 125° detector and around the beamline close to the target chamber. By comparing natural background spectra with and without the shield, a reduction factor of about 20 (6) was determined for the E_γ region around

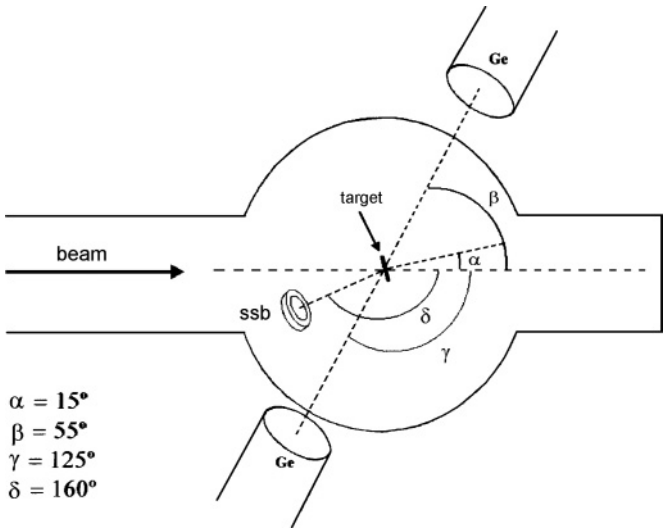

FIG. 2. Experimental setup.

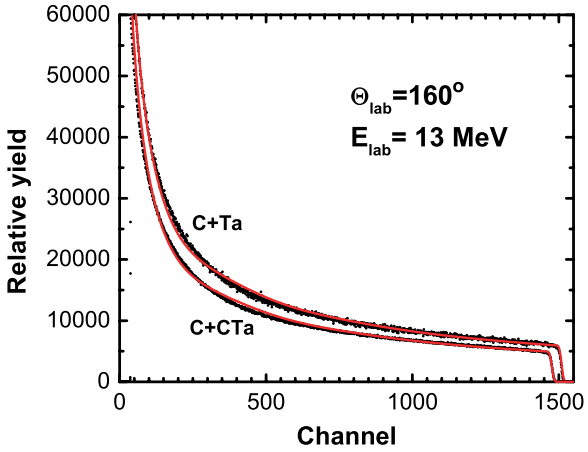

FIG. 3. (Color online) Typical thick-target spectra, obtained at $\theta_{lab} = 160^{\circ}$, at laboratory ^{12}C energy of 13 MeV. Energy calibration is 6.7 keV/channel. Results of bombarding the bare substrate (C + Ta) and the subtrate plus C-foil (C + CTa) are compared.

300 (1500) keV. Because of geometry limitations, the shield for the second detector was only 8 mm thick, but this was not critical since this detector was used mainly to identify the presence of Doppler shift effects. Spectra with no beam were taken both before and after the experiment, indicating no activity contamination of the γ lines of interest. We must mention, however, that these spectra played an important role in properly choosing the integration limits in the case of the 1634 keV line (^{20}Ne) since a background peak was identified close to this line, nearly overlapping the corresponding Doppler shifted component. Whereas inclusion of this peak within the integration interval is probably unimportant for the higher energy points, it would have been disastrous for the lowest energy ones, where the reaction rates are quite low.

Instead of relying on beam-charge collection to get the absolute normalization, as is typical in the standard γ-ray technique, an Silicon Surface Barrier (SSB) detector was placed at 160° in order to measure the ^{12}C ions elastically scattered from the Ta backing. This produces a thick-target spectrum that can be used to determine the absolute normalization factors involving both the target thickness and the integrated number of projectiles [33]. Sample spectra are shown in Fig. 3, obtained at a bombarding energy of 13 MeV for the carbon-plus-substrate and the bare substrate, while the light solid curves were obtained with the simulation code SIMNRA [34]. The height of the plateau is directly related to the number of projectiles, whereas the position of the rapid dropoff depends on the thickness of the carbon foil, in a way that can be determined through kinematic and energy loss calculations. In Fig. 3, the spectrum corresponding to the bare substrate was multiplied by an arbitrary factor for clarity; the observed energy shift between the two spectra characterizes the foil thickness.

Since SIMNRA does not account for possible uncertainties in the energy-loss calculations, a note about the handling of related errors is in order here. A comparison with experimental values of the stopping powers, which SIMNRA calculates according to Ref. [35], shows that the calculation overpredicts the data with a mean error of about 5% for the case of carbon ions [36,37]. For the particular case of ∼1–12 MeV carbon ions in amorphous carbon targets, Paul and Schinner [37] interpreted this as a (negative) systematic error, while the 4.4% spread about the mean is associated with an additional random component. Consistent with this, all target thicknesses obtained with SIMNRA in the present work have been corrected by increasing them by 5% and, in addition, a 4.4% error has been quadratically added to other random errors. The determination of the latter ones has been discussed elsewhere [30].

The silicon detector was calibrated with a triple α source (^{241}Am, ^{244}Cm, ^{239}Pu), and the calibration was monitored with spectra obtained by bombarding the bare Ta backing at five different energies spanning the whole energy region used in the experiment (13, 10.9, 9.85, 9.10, and 8.95 MeV). An unexpected complication arose because the SSB detector presented a fluence-induced pulse-height defect which effectively changed the calibration for the different experimental points. This change, however, occured in a systematic way that could be precisely correlated with the ion fluence at the detector, thus neutralizing the complication. The details of the corresponding analysis have been described in Ref. [38]. In addition, a second SSB detector replaced the original one for the lower energy points starting at 9.85 MeV. Repeat points were taken at this energy with the new detector for both the carbon target and the bare substrate.

The thick-target spectra allowed us to monitor the carbon buildup precisely at the position of the beam spot at the target and thus make the appropriate corrections to both the normalization factor and the reaction energy. It was found that the buildup followed a simple linear behavior with the accumulated number of projectiles, with buildup rates of about 5 ng/cm^2 per particle-μC. Further details of the corresponding analysis have been given in Ref. [30].

A point-to-point normalization was additionally performed by using the 136.1 keV γ line produced by Coulomb excitation of the Ta backing, which should thus have had a smooth excitation function. A smooth curve was generated by fitting the experimental excitation function with a series of Hermite polynomials up to third order, and the ratios of experimental to calculated values were then used to renormalize the points in the excitation functions of interest. This procedure not only guarantees a very good relative normalization for all points obtained with one single target, but also allows one to cross-check the relative target thicknesses of the different carbon foils. A typical correction of about 1% was obtained for the different points, thus indicating that the reported error bars (see below) are most probably overestimated.

The beam energy was calibrated by measuring the excitation function for the ^{12}C(p,p) reaction around the known resonance at 4.808 MeV. To minimize the effects of hysteresis, as a standard procedure we always cycle the magnet up to saturation and take all measurements in a decreasing magnetic field. The radius r of the analyzing magnet was determined within 0.075%; therefore, the energy was known within 0.15%. The consistency of the calibration for the mass-energy region of interest was checked by using the backscattering spectra for 13 MeV C ions from both the bare Ta backing and a thick

Au target. These spectra, taken when the first detector was still free of any pulse-height defect, provided two calibration points for this detector, which were almost perfectly aligned with those obtained from the α source. The errors in the parameters of a linear fit for all five points were quite consistent with the 0.15% uncertainty in the beam energy. Similar results were also obtained for the point at 9.85 MeV on Ta, taken with the second detector. Summarizing, we might say that the beam energy in this experiment was known within ∼15 keV for the lower energies and within ∼20 keV for the higher ones. An energy spread with a standard deviation of about 1.1 keV/MeV is also estimated based on beam optics calculations for the given beam-defining slit system.

Effective beam energies at target were calculated and corrected for both the energy loss and the corresponding variation of the fusion cross section within the target. This variation was determined by interpolating neighboring points with a cubic spline curve, which should thus account for the oscillations of the data. An iterative procedure was followed, similar to the one described in Ref. [39]. The corrections varied between 24 and 53 keV, corresponding to the highest and lowest energy, respectively, with a mean of 35 keV and a standard deviation of 8 keV. Because of the rapid variation of the fusion cross section in the subbarrier region, using it to weigh the energies might actually produce a big effect. In order to emphasize this point, it is worth mentioning that not using it would produce in our case an estimated mean correction of around 100 keV; i.e., all energies would be systematically lower by about 65 keV. This difference, which would increase for thicker targets, might help us understand some of the energy shifts encountered with respect to other works, as shall be described below. As to possible uncertainties in our energy correction, it can be shown that a 5% variation in the target thickness produces only a small effect ($\lesssim$2 keV) on the effective beam energies.

III. EXPERIMENTAL RESULTS

A typical γ-ray spectrum is presented in Fig. 4. A complete identification of peaks has been reported elsewhere [40]. The lines of interest, corresponding to ground-state transitions, are indicated in the figure. As shown, the α, p, and n evaporation channels could be cleanly identified. The lines corresponding to the p and n channels, although separated by only 11 keV, could be resolved despite the Doppler shift component present in both of them. This is better illustrated in the inset of Fig. 4. The ^{20}Ne line also showed a considerable Doppler shift which was properly taken into account during peak integrations. As mentioned in the previous section, the integration limits were carefully set so as to exclude any background contribution.

Fusion residues formed directly in their ground states by particle decay cannot be measured by the γ-ray technique. For the case of neutron evaporation, the yield missed because of this reason can be neglected since the total neutron yield is itself small. In order to estimate the contributions of the α_0 and p_0 channels to the total fusion cross section, the corresponding data on particle measurements in [3,11,24] were carefully compared to each other in the energy region common to the present work. Data in the second and third of these references

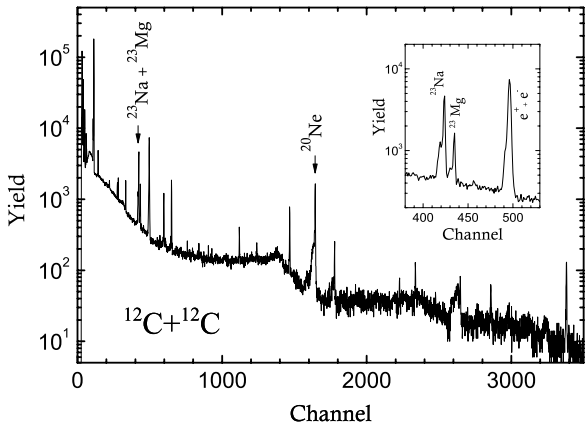

FIG. 4. Typical γ-ray spectrum, obtained with the 125° detector at $E_{\text{c.m.}} = 6.5$ MeV. Inset shows an enlargement of the region containing the lines of interest for the p (^{23}Na) and n (^{23}Mg) channels.

could be said to show good agreement in their energy-overlap region (below $E_{\text{c.m.}} = 5$ MeV), but only if the relative energies are modified by a constant shift of ∼100 keV, for example, shifting them up in [24] (or down in [11]). The data of [3], on the other hand, overlap (in energies) with those of [11] in a wider region (below $E_{\text{c.m.}} = 6.3$ MeV); but in this case, there is no simple transformation that can take one set into the other. Even though the qualitative structure of the data looks very similar, one data set would have to be locally shifted along the energy axis for some bumps while staying unmoved for others in order to reasonably match the other set. The necessary shifts, not larger than ∼30 keV, suggest the existence of nonsystematic errors in the energy, such as would occur in the presence of unknown target thickness variations due to, for example carbon buildup. Notwithstanding this, the absolute cross section values of these ground-state feeding channels are quite similar for the three data sets once the presumed energy errors (systematic or nonsystematic) can be corrected.

Since the positions of maxima and minima in the fusion excitation function of Ref. [11] agree quite well with those in our γ-ray measurements, the above discussion implies that it is reliable to use the α_0 and p_0 cross section values in that reference to correct our data. The correction was made percentagewise or, more specifically, the ratios of $\sigma_{\alpha_0}(E)$ and $\sigma_{p_0}(E)$ to $\sigma_{\text{fus}}(E)$ extracted from Ref. [11] were interpolated with a cubic-spline function and applied to our data. The corresponding contributions for most points were around 5% for each channel, with only one point (5.72 MeV) at which the p_0 correction was above 10% (actually 12%) and five points (4.5–4.74 MeV) at which the α_0 correction was above 10%, with a maximum of 18% for the 4.74 MeV point.

The corrected cross section values obtained for each evaporation channel along with the total fusion cross sections are presented in Table I, and the corresponding excitation functions (uncorrected) are shown in Fig. 5. The error bars in most cases are smaller than the symbol size and include the statistical errors and uncertainties in both the number of projectiles (∼2%) and the target thickness (∼4%). Errors associated with the γ-detector efficiency are also included, but their contribution is generally negligible. As mentioned

TABLE I. Partial and total fusion cross section values for the $^{12}C + {}^{12}C$ system as obtained in this work. The missing yield due to direct ground-state feeding has been corrected for, as explained in the text.

$E_{c.m.}$ (MeV)	σ_α (mb)	Error (mb)	σ_p (mb)	Error (mb)	σ_n (mb)	Error (mb)	σ_{tot} (mb)	Error (mb)
4.42	0.65	0.06	0.25	0.03	0.05	0.02	0.95	0.07
4.5	0.60	0.04	0.26	0.02	0.03	0.01	0.89	0.04
4.59	0.65	0.04	0.38	0.02	0.02	0.01	1.05	0.05
4.66	0.93	0.06	0.54	0.03	0.03	0.01	1.50	0.07
4.74	1.29	0.07	0.76	0.04	0.04	0.01	2.09	0.08
4.82	2.51	0.13	1.44	0.08	0.15	0.02	4.10	0.15
4.89	4.47	0.24	2.32	0.12	0.29	0.04	7.08	0.28
4.88	4.58	0.24	2.74	0.14	0.43	0.03	7.75	0.28
4.96	5.35	0.29	3.64	0.19	0.39	0.03	9.38	0.35
5.03	6.26	0.34	4.18	0.22	0.27	0.03	10.71	0.41
5.1	4.53	0.24	3.38	0.17	0.24	0.03	8.15	0.30
5.19	4.43	0.26	3.34	0.19	0.24	0.03	8.02	0.33
5.26	6.50	0.34	3.78	0.19	0.38	0.03	10.65	0.39
5.34	8.60	0.45	4.45	0.23	0.50	0.05	13.55	0.50
5.42	12.62	0.68	6.12	0.33	1.02	0.08	19.76	0.76
5.49	15.30	0.83	6.14	0.33	1.61	0.11	23.05	0.90
5.57	22.27	1.17	8.63	0.45	1.36	0.11	32.27	1.25
5.64	38.78	2.01	16.76	0.86	2.73	0.18	58.27	2.19
5.72	38.66	1.96	19.50	0.99	2.80	0.19	60.96	2.20
5.79	29.69	1.54	13.60	0.70	1.87	0.15	45.15	1.70
5.87	24.04	1.35	13.49	0.75	2.44	0.15	39.96	1.55
5.95	50.67	2.53	22.68	1.12	5.36	0.30	78.71	2.78
6.02	59.71	2.98	27.58	1.37	4.71	0.28	92.00	3.29
6.1	37.35	1.88	21.77	1.08	3.20	0.20	62.31	2.17
6.17	50.79	2.70	31.08	1.63	3.67	0.23	85.54	3.16
6.25	69.84	4.14	35.09	2.07	3.30	0.24	108.23	4.63
6.32	76.87	3.78	44.52	2.17	4.29	0.24	125.67	4.37
6.4	68.50	3.38	33.59	1.65	4.51	0.25	106.60	3.77
6.48	84.82	4.34	34.90	1.78	7.36	0.43	127.07	4.71

above, the reported error bars most probably overestimate the actual relative errors. An additional 5% systematic error (not included in the error bars) is associated with the solid angle measurement for the SSB detector. The arrows indicate the positions of previously reported resonances in this system, as compiled by Abbondano [41]. Some correlation is apparent between these positions and the bumps in our total cross section data, and this correlation remains when the individual evaporation channels are observed, consistent with true resonances. A parametrization of the data will be attempted below, partially based on these correlations.

IV. CRITICAL REVIEW OF PREVIOUS MEASUREMENTS AND COMPARISON TO OUR DATA

In an effort to establish criteria for data unification, a careful comparison was made between our data and those shown in Fig. 1. By using as a reference the two distinctive bumps in the excitation function around 4.9 and 5.7 MeV, an energy shift ΔE and a scale factor f were introduced when they were needed to make the bumps in a given data set coincide with

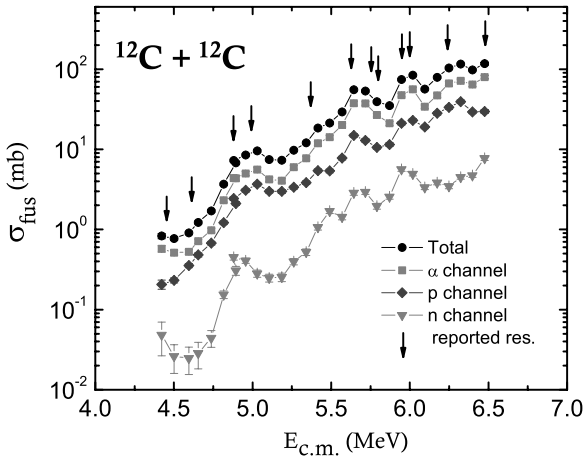

FIG. 5. Excitation functions obtained in this work for the individual fusion-evaporation channels and their sum. No correction for direct population of ground states has been done at this stage.

those in the present work. For data not including both bumps, the corresponding overlap region was compared. The validity of this procedure was partially justified in the introduction when we mentioned the possible consequences of a carbon buildup on the target.

All those data in Fig. 1 that were obtained by using particle techniques were normalized to the elastic scattering yields detected at some forward angle (40° or 45°). This method has the advantage that the product of target thickness times the number of projectiles can be precisely determined, which indeed produces absolute normalization factors with good reliability. The disadvantage is that possible variations in the target thickness itself cannot be detected, and this may lead to imprecisions in the effective reaction energy. Indeed, in the absence of any special provision to prevent carbon buildup, large variations of the target thickness may occur for high enough ion fluences at target [30]. Our hypothesis is that this could explain some of the observed energy shifts between the corresponding data sets. Even though a variable energy shift might in principle be expected from a continuous carbon buildup, we will show that a constant value of ΔE is enough to bring the different excitation functions into near coincidence with each other.

For the case of points obtained with γ-ray techniques, the common feature is that they were all normalized with reference to some previous measurement. Depending on the given reference value, a global scale factor f might be also expected for these points, in addition to a possible ΔE shift.

The main features of the corresponding measurements will be reviewed next, emphasizing those experimental details that might help us understand possible discrepancies. Since for comparison purposes it makes a difference whether the data were published as a table or they had to be read from a figure, this will be indicated for each data set. One should keep in mind that for data read from a plot there might be additional errors due to, for example, image resolution. These errors are estimated to be at most about 10%.

For convenience, we chose to review first the experimental results obtained by using particle techniques. Measurements

using γ-ray techniques, which should in principle be more directly comparable to ours, will then be discussed.

A. Measurements using particle techniques

In 1969, Patterson *et al.* [26] did a very complete measurement of the fusion excitation function for $^{12}C + ^{12}C$, reporting the angle-integrated cross sections in a table. Evaporated protons and α particles were measured at four angles ($20^\circ \leqslant \theta_{lab} \leqslant 80^\circ$) for center-of-mass energies between 3.23 and 8.745 MeV, with 125 keV steps. The neutron channel was deduced, for energies above 4.25 MeV, from the delayed decay of ^{23}Mg. The data were normalized to the elastic scattering measured at 45°. A target thickness of 40 μg/cm^2 is reported, apparently with no special provision to prevent carbon buildup. The data can be brought into close coincidence with ours by applying only a small energy shift, $\Delta E = +20$ keV.

Four years later, in 1973, Mazarakis *et al.* [24] extended the measurements down to $E_{c.m.} = 2.45$ MeV. The data, reported in a table, were obtained with energy steps of about 125 keV for most points, with a maximum energy of 4.91 MeV. Protons and α's were detected at eight angles between 20° and 90°. Elastically scattered carbon nuclei were counted in a detector monitor at 45° for normalization. Self-supporting carbon foils were used as targets, with reported thicknesses of 30 μg/cm^2 for most runs, 53 μg/cm^2 for $E_{c.m.}$ between 2.63 and 2.75 MeV, and 65 μg/cm^2 for the lowest energy point. Again, no mention is made of a possible C buildup on the target, probably indicating that no corresponding provisions were taken. Transformation to our data required in this case a large energy shift, $\Delta E = +100$ keV.

Becker *et al.* (1981) [11] measured angular distributions for the α and p channels for $E_{c.m.}$ between 2.8 and 6.3 MeV using finer steps, i.e., 50 keV. In comparison to the previous works, more angles were measured (a total of nine, $10^\circ \leqslant \theta_{lab} \leqslant 90^\circ$) and thinner targets were used (8–30 μg/cm^2). The combination of target thickness and beam intensity was monitored via the elastic scattering yield observed in the monitor detector at $\theta_{lab} = 40^\circ$. The target thickness was determined to better than 20% and the carbon deposition was estimated to stay below this uncertainty. Lacking further information about the actual C buildup, the authors assigned a conservative 30% uncertainty to the absolute normalization. In spite of this and the fact that these data had to be read from a plot for the astrophysical S factor, quite good agreement was found with our results without having to do any transformation.

The data of Refs. [11,24,26], after the corresponding transformation, are shown in Fig. 6. For comparison, the results of the present work are also included. With few exceptions, the points in the different data sets agree with each other quite nicely. The displayed curves represent model calculations that will be described later.

B. Measurements using γ-ray techniques

The γ-ray measurements of High *et al.* (1977) [25] were done using a thick carbon target, so carbon buildup was not an issue. They used two Ge(Li) detectors placed at ±90° in close geometry. No mention was made in this work about possible γ anisotropies, but the yields for the α and p channels were independently normalized to the particle measurements of Mazarakis and Stephens [24] above 3.5 MeV. The lower energy region, $E_{c.m.} = 2.46$–3.89 MeV, was measured with 125 keV steps, while for $E_{c.m.} = 4.14$–5.88 MeV, the steps were 250 keV. A table with the cross section values was published. Taking into account that the Mazarakis data needed to be shifted by $\Delta E = +100$ keV, a scale factor $f < 1$ could be expected here since the data would have been normalized to overvalued points. Instead, comparison to our results in the common region indicates good agreement if High's data are just shifted up in energy by 75 keV; i.e., for these data, $\Delta E = +75$ keV and no scale factor is needed ($f = 1$).

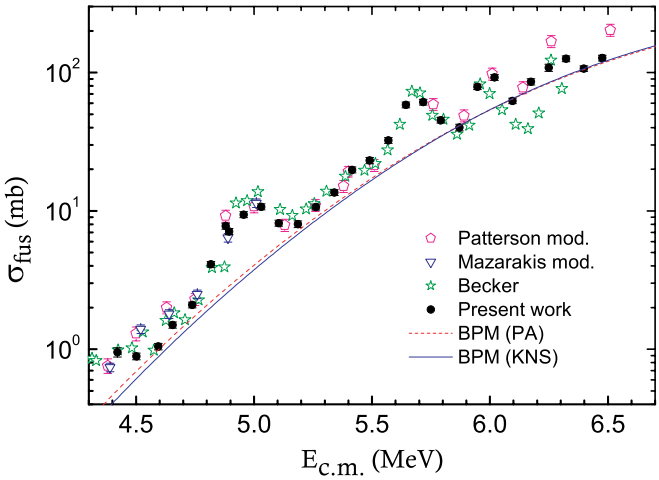

FIG. 6. (Color online) Excitation functions obtained with particle techniques, transformed with the energy shift and the scale factor indicated in the text. Our data are also shown for comparison. The curves are BPM calculations using the proximity adiabatic (PA) and Krappe-Nix-Sierk (KNS) potentials.

Erb *et al.* (1980) [7] measured the excitation function in a higher energy region ($E_{c.m.} = 5.6$–10 MeV) using very fine steps (25 keV). The results were published only as a σ_{fus} vs E plot. A thin carbon foil of 5 μg/cm^2 deposited on a thick gold backing was used as a target and a Ge(Li) detector placed at 90° served to detect the γ rays. Target and backing were biased at +1000 V and surrounded by a mesh biased itself at −1000 V in order to collect the beam charge. An accuracy of 1% was reported in this procedure. The effects of C buildup were monitored by systematic repetition of measurements at selected beam energies; a small effect was observed and corrected for. The decay radiation was found to be nonisotropic for the γ transitions of interest, but the $p + n$ channels were normalized to the Patterson *et al.* data [26] under the implicit assumption that the anisotropies do not change much with energy. A scale factor $f = 0.7$ was enough to make these data coincide with ours in the overlap region, which is consistent with the upward energy shift needed in Ref. [26] (see above). We might say that the attention paid by Erb *et al.* [7]to the carbon buildup on the target is most probably the reason why no energy shift was needed for these data. In fact, even though

not planned this way, the electron suppression biases might have contributed to minimizing the buildup. Indeed, it was shown in Ref. [30] that the amount of C buildup is directly correlated with the number of secondary electrons emitted by the target.

Similar to that in the work of Erb *et al*., a fusion excitation function measured with fine steps (25 keV) was also reported by Kettner *et al*. [9], in this case covering the lower energy region $E_{\text{c.m.}} = 2.45$–6.0 MeV. The γ rays were measured with a Ge(Li) detector at 0° which was surrounded, along with the chamber, by a 7 cm thick lead shield. Carbon targets of 9 to 55 μg/cm^2 were evaporated on a thick Ta substrate. Cross sections obtained with all used targets were normalized to the absolute values of Mazarakis and Stephens for $E_{\text{c.m.}} = 3.80$–4 MeV. γ-ray angular distributions were obtained at 0°, 45°, and 90°, at ten selected beam energies in the range $E_{\text{c.m.}} = 4.0$–6.0 MeV. With few exceptions, they were found to be isotropic or nearly so, a result that contrasts with the above-mentioned anisotropies reported by Erb *et al*., which, on the other hand, might have been measured only at higher energies not overlapping with these last ones. In an effort to prevent C buildup, two cold traps and a 30 cm copper tube placed close to the target were used in Ref. [9], all of them cooled with liquid nitrogen. Considering this, no energy shift was expected for these measurements; instead, transformation to our data required $\Delta E = +50$ keV and $f = 1.35$. We must point out that the authors warn against deducing total fusion cross sections from their measurements in view of existing disagreements in partial cross sections with respect to the Mazarakis and Stephens [24] results. Even though the Kettner *et al*. data [9] were published only as a plot for the astrophysical S factor, they nicely coincide with ours after the transformation. This indicates that the mentioned disagreements are most probably related to the unfortunate situation of normalizing to reference data that actually correspond to different energies.

Dasmahapatra *et al*. [27] used a total-γ-ray-yield method in which all γ rays emitted by fusion residues were detected with two NaI detectors in an almost 4π geometry. In comparison with techniques using Ge detectors, this method has the advantages of increased detection efficiency and independence of the γ-ray angular distribution. The disadvantage is a considerable loss of energy resolution which, for the case of $^{12}C + {}^{12}C$, led these authors to the need of subtracting the 0.511 MeV annihilation peak that overlapped with the γ yields from the ^{23}Na and ^{23}Mg ground-state transitions (see Fig. 4). Measurements were performed in 100–200 keV steps with 30 μg/cm^2 carbon foils, and for absolute normalization the beam charge was collected in a Faraday cup and the elastic scattering was measured with a surface barrier detector at 45°. No provision or estimation is reported in this work to take account of carbon buildup at the target. A small energy shift of $\Delta E = +30$ keV was enough to bring these data, which were read from an S vs $E_{\text{c.m.}}$ plot, into coincidence with ours.

The measurements of Satkowiak *et al*. [12] covered the energy region of $E_{\text{c.m.}} = 5.25$–20 MeV, with steps of 125 keV, and were done with a Ge(Li) detector at 55°. As mentioned above, the effects of possible anisotropies in the γ radiation are minimized for measurements at this angle. A 20 μg/cm^2 carbon foil on a gold backing was used as the target.

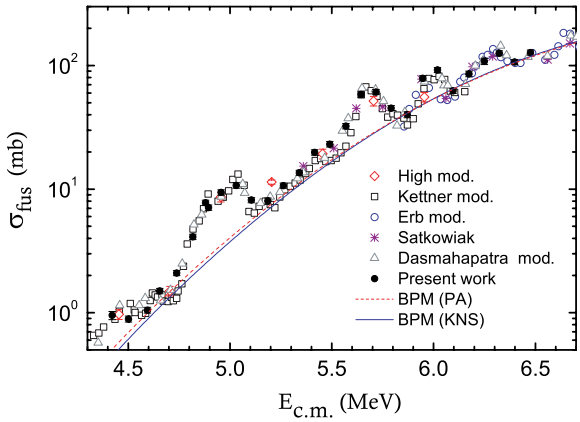

FIG. 7. (Color online) Same as Fig. 6, but for data obtained with γ-ray techniques.

This was completely surrounded by a liquid-nitrogen-cooled shroud with a small beam-entrance aperture, in order to reduce carbon buildup. A relative normalization was derived from Coulomb excitation of Au, and the absolute cross section scale was obtained by normalizing to previous γ-ray data for the same system. The results are in excellent agreement with ours in the common region, without any further transformation.

The whole set of transformed γ-ray data, along with the results of the present work, are displayed in Fig. 7. As can be seen, the proposed transformations bring all different excitation functions to an excellent agreement with each other. The results of this section are summarized in Table II, which gives the transformation parameters for all the reviewed data. It is quite encouraging that the scale factor for most data sets is equal to 1. The obtained ΔE values, however, show compelling evidence that the main source of discrepancies resides in the energy scale. In fact, the origin of the only two exceptions to the $f = 1$ rule can also be traced back to an energy shift in the reference data, as discussed above.

Even though we have discussed possible reasons as to why the various measurements might be shifted in energy, the exact explanation for particular data sets is impossible to assess at this point. The absolute energy scale is therefore still uncertain up to some degree. We might notice, however, that four out of nine independent works (including the present one) show quite good consistency in the energy measurement ($\Delta E = 0$), and one more work (Ref. [26]) is also marginally consistent

TABLE II. Energy shift ΔE and scale factor f proposed to unify the data.

Technique	Ref.	ΔE (keV)	f
Particle	[26]	20	1
	[24]	100	1
	[11]	0	1
γ ray	[25]	75	1
	[9]	50	1.35
	[7]	0	0.7
	[27]	30	1
	[12]	0	1

according to our reported energy errors. It is thus reasonable to adopt the associated energy scale as the most probable one. Supported by this and the previous discussions, which led to Figs. 6 and 7, a data unification is proposed, on the basis of the transformations in Table II. It will be seen below that with this proposal, a reasonable unification is also achieved in the lower energy region, far below our measurements.

V. BARRIER FEATURES AND RESONANCE PARAMETERS

For nonoverlapping resonances, it has been shown that under certain conditions thought to be satisfied by the $^{12}C + ^{12}C$ system, the total reaction cross section does not contain interference effects due to "normal" compound nuclear states [42]. Under these assumptions, the effect on fusion of resonances in the elastic channel can be estimated by adding a sum of Lorentzian (Breit-Wigner) terms to the smooth absorption background cross section $\sigma_{bkg}(E)$ obtained from a mean field potential [7,43].

$$\sigma_{fus}(E) = \sigma_{bkg}(E) + \sigma_{BW}(E), \tag{1}$$

$$\sigma_{BW}(E) = \frac{\pi}{k^2}\sum_{\mu}(2l_\mu + 1)\frac{\Gamma^\mu_{el}\left(\Gamma^\mu_{tot} - \Gamma^\mu_{el}\right)}{(E - E^\mu)^2 + \left(\frac{1}{2}\Gamma^\mu_{tot}\right)^2}, \tag{2}$$

where l_μ, E^μ, Γ^μ_{el} and Γ^μ_{tot} are the angular momentum, the energy, the width for decay to the elastic channel, and the total width, respectively, for the resonance labeled μ.

In the absence of information concerning the behavior of the background term, only lower limits can be established for $\Gamma^\mu_{el}/\Gamma^\mu_{tot}$ [7]. Consequently, in most cases the resonance widths that can be extracted from fusion data are only poorly known. Knowledge of these parameters is, of course, important when discussing the ^{12}C clustering in the doorway states leading to fusion. In this work, $\sigma_{bkg}(E)$ will be estimated from the one-dimensional barrier penetration model (BPM). The respective curve should actually represent a background rather than a mean value for the excitation function, since $\sigma_{BW}(E)$ is nonnegative. The potential barrier is described by a nuclear and a Coulomb contribution

$$V(r) = V_N(r) + V_C(r), \tag{3}$$

$$V_C(r) = \begin{cases} \dfrac{[3 - (r/R_C)^2]Z_pZ_te^2}{2R_C} & r < R_C, \\ \dfrac{Z_pZ_te^2}{r} & r \geqslant R_C, \end{cases} \tag{4}$$

with Z_p, Z_t being the atomic numbers of projectile and target, respectively, and R_C the Coulomb radius defined by

$$R_C = 1.3\left(A_p^{1/3} + A_t^{1/3}\right). \tag{5}$$

Five different options were tried for the (real) nuclear potential $V_N(r)$ by fitting the background in our data: Woods-Saxon (WS) [44], proximity-adiabatic (PA) [45], proximity-sudden (PS) [45], Krappe-Nix-Sierk (KNS) [46], and Ngo [47]. The transmission coefficient for the l-th partial wave, $T_l(E)$, was calculated within the WKB approximation [48] for energies below the corresponding effective barrier and from the Hill-Wheeler formula [49] otherwise. The fusion cross section is given by

$$\sigma_{BPM}(E) = 2\pi\lambda\!\!\!^{-2}\sum_{l=\text{even}}^{\infty}(2l + 1)T_l(E), \tag{6}$$

where the identity of the particles has been taken into account. Only one free parameter was used for each potential, related to the well depth in the case of the Woods-Saxon potential and to the respective radius for all the remaining ones. The five potentials gave similar curves for the cross sections in the energy region of our data, but with slightly different slopes. When the calculations were extended down to the lower limit of other existing measurements, however, the KNS potential gave the most reasonable reproduction of data. Both the adiabatic and the sudden approximations to the proximity potential produced equivalent results, overpredicting the experimental background. The WS and NGO potentials overpredicted even further the data in the low energy end.

The barriers generated by the different nuclear potentials are illustrated in Fig. 8 and the corresponding parameters

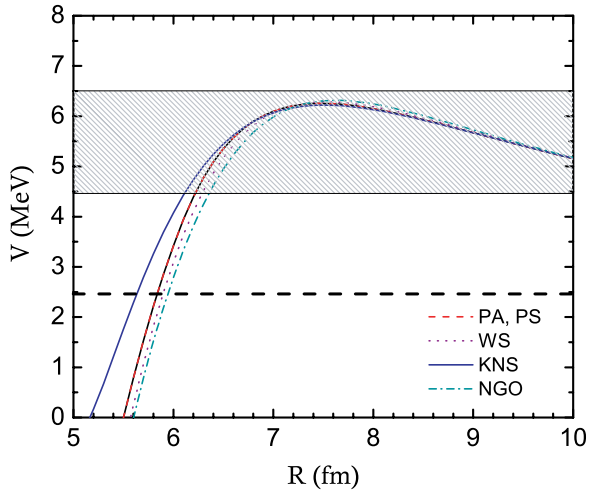

FIG. 8. (Color online) One-dimensional barriers [Eq. (3)] generated by the different nuclear potentials for $^{12}C + ^{12}C$. Shadowed area represents the energy region of our measurements; horizontal dashed line indicates the lowest energy for which experimental fusion data exist. Above 10 fm, the interaction is essentially Coulomb, regardless of the nuclear potential.

TABLE III. Fusion barrier parameters obtained from fitting the background in our data with Eq. (6), using the different nuclear potentials mentioned in the text.

Potential	V_0 (MeV)	R_0 (fm)	$\hbar\omega$ (MeV)
KNS	6.23	7.49	2.58
PA,PS	6.27	7.47	2.70
Ngo	6.33	7.60	2.95
WS	6.30	7.52	2.83

are given in Table III. The barrier height turns out to be fairly independent of the chosen potential, consistent with the results reported in Ref. [50], where a similar procedure was followed to fit above-barrier data for a variety of systems. At the lowest measured energies (about 2.5 MeV), however, the horizontal dashed line in Fig. 8 clearly shows that a barrier region is being probed for which the chosen nuclear potential does make a difference. So, low-energy fusion cross sections can certainly help to determine the interior of the potential, thus complementing elastic scattering data, which are well known to be sensitive mostly to the surface region. This feature is expected to be useful in reducing ambiguities in optical potentials at subbarrier energies. Work aimed at extending the existing optical model analyses to these lower energies is currently in progress [18].

Since the ^{12}C nucleus is oblate deformed in its ground state, the fitted BPM potential should represent some kind of average effect for the interaction of the deformed nuclei with different relative orientations. In fact, in order for the resonant doorway states leading to fusion to be favored, it should mainly represent the situation where the nuclei approach each other with their axes of symmetry perpendicular to the line of approach [51,52] (see also [53], p. 627). Our results indicate that this situation is well represented by the KNS potential. We may also notice that the barrier heights reported in Table III are in fact consistent with this belly-to-belly orientation of the nuclei at the touching point [52].

Using our data for $\sigma_{\rm fus}(E)$ and setting $\sigma_{\rm bkg}(E) = \sigma_{\rm BPM}(E)$ for the KNS potential, a fit was done to $\sigma_{\rm fus}(E) - \sigma_{\rm bkg}(E)$ with expression (2). Resonance parameters for the region of interest have been reported in the literature [2,3,7,13,41,54–56], from which energies and angular momenta were taken. However, some of these energies were varied within the reported uncertainties in order to better fit the data. Estimations for total widths and for a few elastic widths have also been given in the same references, but they were taken mainly as a guide for the present fit, varying them manually until a good description of the whole data set was obtained. Since the presence of a resonance affects its neighbors, three reported resonances lying out of (but near) the measured energy region were also included. In addition, the energy dependence of the widths, which is important in the subbarrier region (Ref. [53], p. 242), was assumed to be described by multiplying the constant $\Gamma_{\rm el}^{\mu}$ times $T_l(E)/T_l(E^{\mu})$, where l is the angular momentum of the resonance.

The resulting fit is displayed in Fig. 9, where the single Lorentzians are also illustrated, and the corresponding resonance parameters are presented in Table IV. In order to emphasize the fact that resonances corresponding to different angular momenta do not interfere they have been classified according to their l value in both the figure and the table. Since the spacing between successive resonances with the same l is always larger than the corresponding widths, the assumption of nonoverlapping resonances should produce a fairly good approximation. Two things should be clarified at this point. First, the peak around 5.66 MeV, previously reported as a broad-resonance with a total width above 100 keV [3,54], was split into two narrower resonances (5.66 and 5.71 MeV) with different angular momenta. The existence

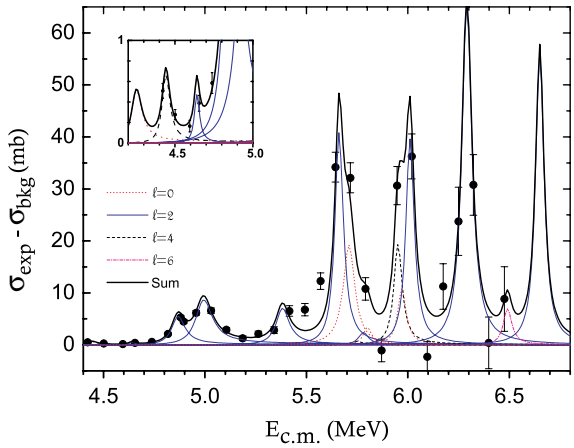

FIG. 9. (Color online) Fusion resonances after background subtraction (KNS potential) and the result of the fit with Eq. (2) corresponding to the parameters of Table IV. Individual Breit-Wigner terms are also shown.

TABLE IV. Resonance parameters obtained from fitting $\sigma_{\rm exp} - \sigma_{\rm bkg}$ with Eq. (2), where $\sigma_{\rm bkg}$ was calculated using the KNS potential in the BPM. Resonances centered at 4.25, 6.49, and 6.65 MeV fall out of our experimental energy region, but their tail's effect was considered.

This work			Previous work				
E (MeV)	$\Gamma_{\rm el}$ (keV)	$\Gamma_{\rm tot}$ (keV)	l	E (MeV)	$\Gamma_{\rm el}$ (keV)	$\Gamma_{\rm tot}$ (keV)	Ref.
4.25	0.4	80	0	4.25		60–80	[3]
(5.71)	35	70	(0)				[3]
5.80	2.37	50	0	5.82		50	[13]
5.97	9.0	50	0	5.97		50	[13]
4.64	0.04	40	2	4.62		60–80	[3]
4.865	1.0	80	2	4.88		80	[3]
4.99	2.0	100	2	5.00		60–80	[3]
5.38	1.4	80	2	5.37		60–80	[3]
5.66	6.0	50	2	5.64		140	[3]
			2	5.6	20	104	[54]
			2	5.6	10	130	[55]
5.78	0.38	60	2	5.8		60	[13]
6.01	6.2	50	2	6.01		70	[13]
6.29	15	60	2	6.25		60–80	[3]
				6.28	$\geqslant$16	125	[7]
6.65	11	50	2	6.64	29	100	[55]
				6.63	40	100	[7]
4.44		60	4	4.46		60–80	[3]
	0.045						
5.75	0.06	60	4	5.77		60	[13]
5.95	1.5	50	4	5.92	4	60	[3]
				5.96	$\geqslant$3	100	[7]
			4	5.94		50	[13]
					3.75		
			4	6.0	7.5	88	[54]
			4	6.0	4	100	[55]
6.49	0.4	50	(6)	6.49		$\geqslant$50	[7]

of a second unresolved resonance, with $l = 0$, was in fact suspected in Ref. [3]. The present results are consistent with this, since using a single broad resonance in our analysis would affect too much the neighboring ones, making it impossible to get a reasonable global fit. The widths reported in Table IV for the 5.71 MeV resonance should be taken with due reserve, as they are conditioned to the validity of the $l = 0$ assumption.

Second, the three resonances reported in Ref. [13] at 5.77 MeV ($l = 4$), 5.80 ($l = 2$), and 5.82 ($l = 0$), are obviously too close together as to extract independent parameter values for each of them out from our data. Instead, $\Gamma_{\rm el}$ ratios consistent with the *S*-matrix moduli of that reference were fixed and only one parameter was fit to our data. (The $\Gamma_{\rm tot}$ values of Ref. [13] were not changed.) In the process, a small systematic energy shift (−20 keV) was found to improve the consistency with our data. Notice that interference effects that could appreciably change the Lorentzian shapes should not be expected here since the three resonances have different angular momenta.

An important issue is the possible sensitivity of the resonance parameters to the used background. We investigated this by doing in addition a fit similar to the one in Fig. 9 but using for the background the PA (or PS) potential. As a result, all parameters in columns 2 and 3 of Table IV remained unchanged, except for a few of the lower energy resonances, where small modifications occurred. A maximum variation of 0.7 keV in the elastic width and 20 keV in the total width was observed, which is well within the experimental uncertainties. In addition, we shall see below that the lowest energy points in the unified data seem to favor the background generated by the KNS potential, so we may say that the parameters reported in Table IV are also favored. The sensitivity to a systematic 5% change in the cross sections was also tested. Only a few of the $\Gamma_{\rm el}$ values changed, with variations between 0.01 and 1 keV, while only one $\Gamma_{\rm tot}$ value had to be modified, by 10 keV.

We emphasize that the parameters in Table IV were not obtained from our data starting from scratch; this would not be feasible given the limited number of points and the fact that the resonance spin cannot be determined unambiguously from fusion data. Instead, the existent information was adapted, within reported uncertainties, to make it consistent with the present results. This approach must be validated by comparing the predictions to a more complete set of data. This is done in Fig. 10, where they are compared to some unified cross section data. Later on, the corresponding predictions for the astrophysical *S* factor will be compared with the whole set of unified data. We may conclude that the constraints imposed by total fusion measurements can certainly help determine resonance parameters, thus complementing other observations.

In spite of much theoretical effort to explain the observed resonances [14,53,57–59], a sound model with quantitative predictions is still missing. The parameters of Table IV, which take into account the contribution of each resonance to the whole energy region, should establish a better ground for testing any relevant model. More work aimed at a theoretical description of the resonances is currently in progress [60,61].

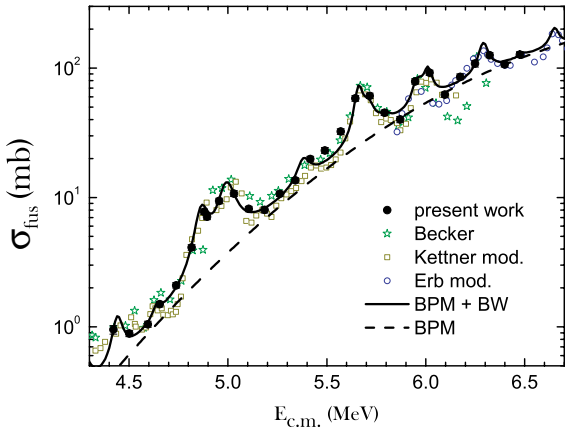

FIG. 10. (Color online) Some unified cross section data and predictions of Eq. (1) using the BPM with the KNS potential to calculate $\sigma_{\rm bkg}(E)$ and the resonance parameters of Table IV to calculate $\sigma_{\rm BW}(E)$.

VI. EXTRAPOLATION TO LOW ENERGIES

For energies far below the barrier, the dominant effect is given by the Coulomb forces. Therefore, data in this region are usually discussed in terms of the astrophysical *S* factor, which factors out the Coulomb effects, separating them from the nuclear part. The expression we use for the *S* factor, appropriate for the $^{12}C + {}^{12}C$ system [9,24,26], is given by

$$S = \sigma E_{\rm c.m.} \exp\left(87.21 E_{\rm c.m.}^{-1/2} + 0.46 E_{\rm c.m.}\right), \qquad (7)$$

with $E_{\rm c.m.}$ given in units of MeV. A plot of *S* vs $E_{\rm c.m.}$ is given in Fig. 11 for the whole unified data at subbarrier energies. It can be seen that if the reported uncertainties are taken into account, the proposed unification has removed most of the existing discrepancies, even for the lowest energy points lying below the region measured in this work. The BPM curves corresponding to the KNS and PA potentials are also displayed, as well as the Breit-Wigner fit of Fig. 9, this last one only for its respective region of validity. Apparently, the KNS-based curve gives a better background description at the lowest energies. The extrapolated curves predict background values of *S* in the region of astrophysical interest (1–3 MeV) with an average of about $1.13(1.64) \times 10^{16}$ MeV b for the KNS (PA) potential.

Since fluctuations in *S* seem to persist even at the lowest energies, the actual values of *S* in that region cannot be predicted, but the extrapolated curves could be taken as lower bound estimations. Along with the unified data shown, they should give quite a good estimation of the average *S* for the purpose of doing relevant astrophysical calculations. It would be interesting, though, to make lower energy measurements that could extend the existing data and decrease the uncertainties. Efforts in this direction have been done lately [62,63], and new results are expected soon. On the theoretical side, it is important to develop better models capable of properly describing the observed fluctuations and having predictive power. As mentioned above, some work in this direction is presently in progress [60,61].

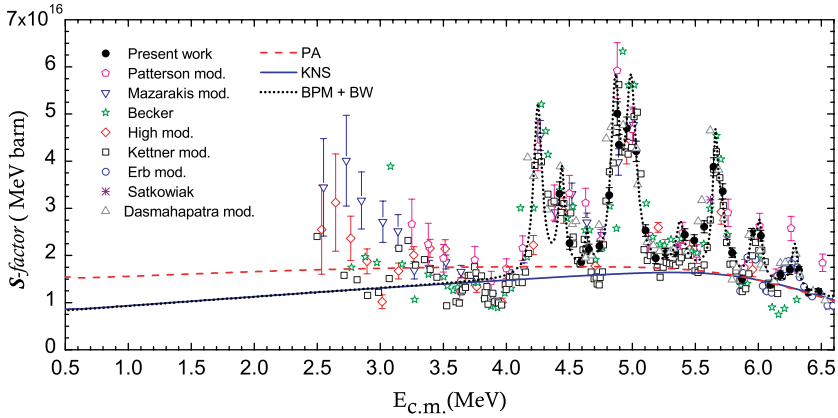

FIG. 11. (Color online) Energy dependence of the astrophysical S factor calculated for all data sets after unification. Smooth curves are the BPM predictions for the KNS (solid) and PA (dashed) potentials. Breit-Wigner fit of Fig. 9 is also shown.

VII. SUMMARY AND CONCLUSIONS

Excitation functions were measured for all fusion-evaporation channels of the $^{12}C + {}^{12}C$ reaction in the region between 4.42 and 6.48 MeV in the center-of-mass system. The γ-ray technique was used with a new normalization method that allows a simultaneous determination of both the number of incident projectiles and the target thickening produced by carbon buildup.

Eight previously reported experiments, containing fusion measurements in energy regions overlapping with ours, were carefully reviewed and compared to the present results. The main source of discrepancies was found to be the absolute energy scale. Very good overall agreement, both in energy scale and in absolute cross sections, was observed with two of these reports [11,12], and in two more works the energy scale was consistent with ours within the reported uncertainties [7,26]. After doing a simple transformation that can probably be ascribed to either a lack of accurate information about the carbon buildup on target or to possible imprecisions in the reaction-energy determination, all the rest of the reviewed data could be brought into reasonable coincidence, thus leading to a proposed unification of data. Implicit in this proposal is the choice of an absolute energy scale based upon agreement between the largest number of independent measurements.

Structure is observed in the excitation function which is consistent with previously reported resonances in this system. Starting from reported values, a new set of resonance parameters is obtained by choosing a reasonable background and doing a simultaneus fit to all resonances in the region of our data. A sum of Breit-Wigner terms is used for the resonant part, with energy-dependent partial widths. The new parameters thus include an approximate account of the influence of any given resonance on its neighbors. As an outcome, the previous information is not only modified but also complemented by adding a consistent set of partial widths for the elastic channel. A more rigorous treatment describing possible interference effects between resonances is, of course, desirable, but falls beyond the scope of the present work.

Of the four real potentials tried within the barrier penetration model, the Krappe-Nix-Sierk potential [46] gave the most reasonable description of the experimental background. As a side conclusion, we may say that the global behavior of the $^{12}C + {}^{12}C$ system is normal, i.e., the BPM with a properly chosen one-dimensional potential is able to describe the data trend quite well. The corresponding fusion barrier is consistent with that expected for two oblate ^{12}C nuclei oriented belly-to-belly at the touching point, in agreement with theoretical predictions [51,52]. On this basis, the validity of the BPM descriptions to extrapolate to the region of astrophysical interest was discussed.

Further measurements with our technique, extending to the lower energy region relevant to the carbon burning process in aging massive stars, are feasible and desirable.

ACKNOWLEDGMENTS

Thanks are due to Pedro Villaseñor and Gaudencio Linarte for their valuable help in keeping the accelerator running during the experiment. One of the authors (EFA) aknowledges fruitful discussions with Peter Hess, Joaquin Gomez Camacho, and Antonio Moro. This work was partially supported by the CONACYT (Mexico).

[1] D. A. Bromley, J. A. Kuehner, and E. Almquist, Phys. Rev. Lett. **4**, 365 (1960).
[2] E. Almquist, D. A. Bromley, and J. A. Kuehner, Phys. Rev. Lett. **4**, 515 (1960).
[3] W. Galster, W. Treu, P. Duck, H. Frohlich, and H. Voit, Phys. Rev. C **15**, 950 (1977).
[4] R. Wada, J. Schimizu, and K. Takimoto, Phys. Rev. Lett. **38**, 1341 (1977).
[5] J. J. Kolata, R. M. Freeman, F. Haas, B. Heusch, and A. Gallmann, Phys. Rev. C **21**, 579 (1980).
[6] J. J. Kolata, R. E. Malmin, P. A. DeYoung, S. Davis, and R. Luhn, Phys. Rev. C **21**, 776 (1980).
[7] K. A. Erb, R. R. Betts, S. K. Korotky, M. M. Hindi, P. P. Tung, M. W. Sachs, S. J. Willett, and D. A. Bromley, Phys. Rev. C **22**, 507 (1980).
[8] W. Treu, H. Frohlich, W. Galster, P. Duck, and H. Voit, Phys. Rev. C **22**, 2462 (1980).
[9] K. U. Kettner, H. Lorenz-Wirzba, and C. Rolfs, Z. Phys. A **298**, 65 (1980).

[10] A. M. Nathan, A. M. Sandorfi, and T. J. Bowles, Phys. Rev. C **24**, 932 (1981).
[11] H. W. Becker, K. U. Kettner, C. Rolfs, and H. P. Trautvetter, Z. Phys. A **303**, 305 (1981).
[12] L. J. Satkowiak, P. A. DeYoung, J. J. Kolata, and M. A. Xapsos, Phys. Rev. C **26**, 2027 (1982).
[13] Z. Basrak, W. Tiereth, N. Bischof, H. Frohlich, B. Nees, E. Nieschler, and H. Voit, Phys. Rev. C **32**, 910 (1985).
[14] W. Greiner, J. Y. Park, and W. Scheid, *Nuclear Molecules* (World Scientific, Singapore, 1995).
[15] M. E. Brandan, M. Rodríguez-Villafuerte, and A. Ayala, Phys. Rev. C **41**, 1520 (1990).
[16] K. W. McVoy and M. E. Brandan, Nucl. Phys. **A542**, 295 (1992).
[17] Y. Kondo, M. E. Brandan, and G. R. Satchler, Nucl. Phys. **A637**, 175 (1998).
[18] T. L. Belyaeva, E. F. Aguilera, and R. Pérez-Torres, Rev. Mex. Fís. **50** S2, 11 (2004); in Book of Abstracts of the International Nuclear Physics Conference, INPC2004, Göteborg, Sweden, June 27–July 2, 2004, p. 444 (unpublished).
[19] Shiu-Chin Wu, Shyh-Jen, and Shen-Haw Chiou, Nucl. Phys. **A570**, 387c (1994).
[20] F. Kappeler, F. K. Thielemann, and M. Wiescher, Annu. Rev. Nucl. Part. Sci. **48**, 175 (1998).
[21] A. N. Ostrowski, T. Davison, K. Fohl, M. Seidl, and H. Voit, Nucl. Phys. **A688**, 130 (2001).
[22] M. Beard and M. Wiescher, Rev. Mex. Fís. **49** S4, 139 (2003).
[23] L. R. Gasques, A. V. Afanasjev, E. F. Aguilera, M. Beard, L. C. Chamon, P. Ring, M. Wiescher, and D. G. Yakovlev, Phys. Rev. C **72**, 025806 (2005).
[24] M. G. Mazarakis and W. E. Stephens, Phys. Rev. C **7**, 1280 (1973).
[25] M. D. High and B. Cujec, Nucl. Phys. **A282**, 181 (1977).
[26] J. R. Patterson, H. Winkler, and C. S. Zaidinis, Astrophys. J. **157**, 367 (1969).
[27] B. Dasmahapatra, B. Cujec, and F. Lahlou, Nucl. Phys. **A384**, 257 (1982).
[28] G. Blondiaux, M. Valladon, L. Quaglia, G. Robaye, G. Weber, and J. L. Debru, Nucl. Instrum. Methods **227**, 19 (1984).
[29] M. J. F. Healy, Nucl. Instrum. Methods B **129**, 130 (1997).
[30] E. F. Aguilera, P. Rosales, E. Martinez-Quiroz, G. Murillo, and M. C. Fernández, Nucl. Instrum. Methods B **244**, 427 (2006).
[31] P. Rosales, E. F. Aguilera, E. Martinez-Quiroz, G. Murillo, R. Policroniades, A. Varela, E. Moreno, M. Fernández, H. Berdejo, J. Aspiazu, D. Lizcano, H. García-Martínez, A. Gómez Camacho, E. Chávez, M. E. Ortiz, A. Huerta, and R. Macías, Rev. Mex. Fís. **49** S4, 88 (2003).
[32] E. F. Aguilera, Rev. Mex. Fís. **43**, 600 (1997).
[33] E. F. Aguilera, E. Martinez-Quiroz, H. M. Berdejo, and M. C. Fernández, Rev. Mex. Fís. **41**, 507 (1995).
[34] M. Mayer, Max-Planck-Institut fur Plasmaphysik, Garching, Germany, Report IPP 9/113, SIMNRA User's Guide, 1997 (unpublished).
[35] J. F. Ziegler, J. P. Biersack, and U. Littmark, *The Stopping and Range of Ions in Solids, Vol. 1* (Pergamon Press, New York, 1985).
[36] J. F. Ziegler, computer code SRIM version 2003, http://www.srim.org/.
[37] H. Paul and A. Schinner, Nucl. Instrum. Methods B **209**, 252 (2003).
[38] E. F. Aguilera, P. Rosales, and F. J. Ramírez-Jiménez, IEEE Trans. Nucl. Sci. **52**, 1785 (2005).
[39] E. F. Aguilera, J. J. Vega, J. J. Kolata, A. Morsad, R. G. Tighe, and X. J. Kong, Phys. Rev. C **41**, 910 (1990).
[40] P. Rosales, Masters thesis, Universidad Nacional Autónoma de México (UNAM), 2005, (unpublished).
[41] U. Abbondano, Trieste Report No. INFN/BE-91/11, 1991 (unpublished).
[42] H. Frohlich, P. Duck, W. Treu, and H. Voit, in *Resonances in Heavy-Ion Reactions*, edited by K. A. Eberhard, Lecture Notes in Physics, Vol. 156 (Springer Verlag, Berlin, 1982), p. 79.
[43] S. Y. Lee, H. W. Wilschut, and R. Ledoux, Phys. Rev. C **25**, 2844 (1982).
[44] P. R. Christensen and A. Winther, Phys. Lett. **B65**, 19 (1976); R. A. Broglia and A. Winther, *Heavy Ion Reactions* (Benjamin, New York, 1981), Vol. I, p. 114.
[45] J. Blocki and W. J. Swiatecki, Ann. Phys. (NY) **132**, 53 (1981).
[46] H. J. Krappe, J. R. Nix, and A. J. Sierk, Phys. Rev. C **20**, 992 (1979).
[47] H. Ngo and Ch. Ngo, Nucl. Phys. **A348**, 140 (1980).
[48] M. Beckerman, Rep. Prog. Phys. **51**, 1047 (1988).
[49] D. L. Hill and J. A. Wheeler, Phys. Rev. **89**, 1102 (1953).
[50] L. C. Vaz, J. M. Alexander, and G. R. Satchler, Phys. Rep. **69**, 373 (1981).
[51] M. Harvey, in *Proceedings of the Second International Conference on Clustering Phenomena in Nuclei, College Park 1975*, (USDERA Report ORO-4856-26), p. 549.
[52] P. O. Hess, J. Schmidt, and W. Scheid, Ann. Phys. (N.Y.) **240**, 22 (1995).
[53] H. Feshbach, *Theoretical Nuclear Physics. Nuclear Reactions* (Wiley, New York, 1992).
[54] E. Almqvist, D. A. Bromley, J. A. Kuehner, and B. Whalen, Phys. Rev. **130**, 1140 (1963).
[55] S. K. Korotky, K. A. Erb, S. J. Willett, and D. A. Bromley, Phys. Rev. C **20**, 1014 (1979).
[56] K. A. Erb and D. A. Bromley, Phys. Rev. C **23**, R2781 (1981).
[57] K. A. Erb and D. A. Bromley, in *Treatise on Heavy-Ion Science*, edited by D. A. Bromley (Plenum, New York, 1985), Vol. 3, p. 201.
[58] P. O. Hess and P. Pereyra, Phys. Rev. C **42**, 1632 (1990).
[59] P. O. Hess, A. Algora, J. Cseh, and J. P. Draayer, Phys. Rev. C **70**, 051303(R) (2004).
[60] P. O. Hess, P. Rosales, E. F. Aguilera, A. Algora, J. Cseh, J. P. Draayer, and T. L. Belyaeva, in *Proceedings of the International Symposium on Exotic Nuclear Systems, Debrecen, Hungary, June 20–25, 2005*, AIP Conf. Proc. Vol. 802, edited by Z. Gácsi, Zs. Dombrádi, and A. Krasznahorkay (AIP, New York, 2005), p. 69.
[61] P. O. Hess, E. F. Aguilera, E. Martinez-Quiroz, A. Algora, J. Cseh, J. P. Draayer, and T. L. Belyaeva, Acta Phys. Hung. A (2006) (to be published).
[62] L. Barrón-Palos, E. Chávez, A. Huerta, M. E. Ortiz, G. Murillo, E. F. Aguilera, E. Martinez-Quiroz, E. Moreno, R. Policroniades, and A. Varela, Rev. Mex. Fís. **50** S2, 18 (2004).
[63] L. Barrón-Palos, E. Chávez, A. Huerta, M. E. Ortiz, G. Murillo, E. F. Aguilera, E. Martinez-Quiroz, E. Moreno, R. Policroniades, and A. Varela, Eur. Phys. J. A **25**, 645 (2005).